The Detuning Effects of a Wrist-Worn Antenna and Design of a Custom Antenna Measurement System

John Buckley[1], Kevin G. McCarthy[2], Brendan O'Flynn[1], Cian O'Mathuna[1]

[1]*Tyndall National Institute, Lee Maltings, Prospect Row, Cork, Ireland*

[1]john.buckley@tyndall.ie

[2]*Department of Electrical and Electronic Engineering, University College Cork, Ireland*

[2]k.mccarthy@ucc.ie

***Abstract*—This paper investigates the effects of antenna detuning on wireless devices caused by the presence of the human body, particularly the wrist. To facilitate repeatable and consistent antenna impedance measurements, an accurate and low cost human phantom arm, that simulates human tissue at 433MHz frequencies, has been developed and characterized. An accurate and low cost hardware prototype system has been developed to measure antenna return loss at a frequency of 433MHz and the design, fabrication and measured results are presented. This system provides a flexible means of evaluating closed-loop reconfigurable antenna tuning circuits for use in wireless mote applications.**

I. Introduction

Wearable wireless technology is seeing a rapid emergence in recent times in areas such as healthcare and activity monitoring, driven by the need for small and reliable monitoring devices. This technology can be used in applications such as out-patient monitoring and providing in-home lifelines for the elderly [1-2]. Wireless sensor motes [3] are an ideal platform for these types of applications.

When wireless devices including motes, are placed close to the human body, the electromagnetic coupling between antenna and body can affect antenna parameters such as impedance, efficiency, radiation and polarization characteristics [4-5]. In this work, the target system is a modular wireless mote that operates in the 433MHz frequency band which has favourable on-body propagation characteristics. The investigation focuses on the degree of antenna impedance variation caused by the presence of the human wrist. Antenna impedance mismatch causes a reduction in radiated power and therefore, the transmitter power needs to be increased to maintain the original radiated power level, leading to increased power consumption and reduced battery lifetime. One solution to this problem is to employ an impedance matching network to correct for the variations in antenna impedance. The design of a suitable matching network requires accurate knowledge of the range of antenna impedances that are possible in practice. It is difficult to obtain consistent antenna impedance measurement in practice using real human bodies due to problems of movement, repeatability and traceability. Accurate phantoms that mimic the human body are commercially available but are expensive. An alternative approach is presented here in the development and characterization of a low cost human phantom, using readily available materials. A low cost hardware prototype system has been developed to measure antenna return loss in real time and display the results on a GUI. The measured results for the prototype system are compared to those using traditional vector network analyser (VNA) measurements. The system provides a flexible platform for design and testing of reconfigurable antenna tuning circuits.

II. Antenna Detuning

The detuning effects of the human wrist were first investigated by measuring the return loss of a chosen test antenna in free-space and then on the human wrist. The test antenna is a commercial 433MHz, 50Ω planar type [6], mounted on a 25 x 25mm printed circuit board as shown in Figure 1. The antenna is fed by an SMA connector and 50Ω co-planar waveguide, printed on an FR-4 substrate of thickness 1.52 mm, permittivity 4.5, and loss tangent of 0.02. The measured results are shown in Figure 2.

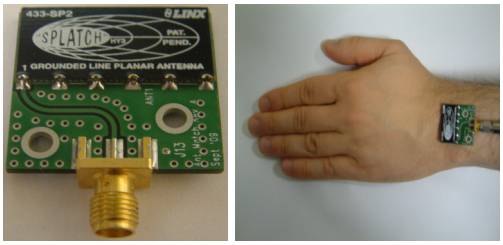

Fig. 1 Test antenna assembly and antenna on human wrist

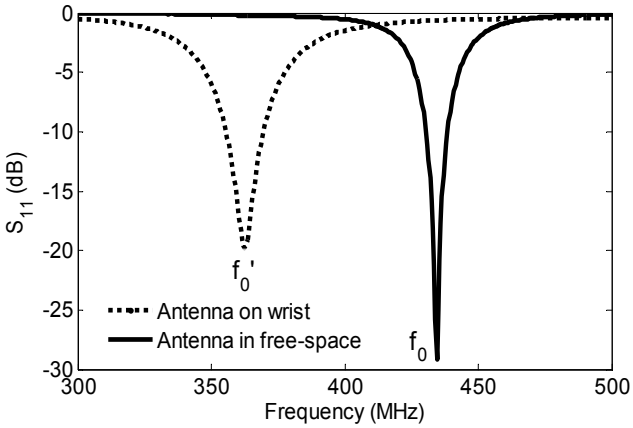

Fig. 2 Antenna detuning caused by human wrist

It can be seen that in free-space, the antenna is correctly tuned at a frequency f_0 of 433MHz with a return loss of close to 30dB. When the antenna is then placed on the human wrist, touching the skin, the resonant frequency decreases to a value of 363MHz with almost 30dB decrease in return loss at f_0 and this represents a very large impedance mismatch with a VSWR of almost 8:1. This detuning is attributed to the change in antenna impedance from approximately 43.81-j24 Ω in free-space to a value of 45.7+j122.1Ω when the antenna is placed on the human wrist.

III. Phantom Arm Design & Characterization

Different materials have been used to simulate human tissue materials at microwave frequencies [7-8]. One approach uses a sucrose (sugar) and saline solution where the ingredients are inexpensive and readily available. These liquids can provide an accurate equivalent of the dielectric properties, particularly the relative permittivity and conductivity of human tissue over a certain frequency range. The sucrose ingredient is used to control the permittivity of the solution while sodium chloride is used to control conductivity. For this study, the proportions (by weight) of water, sucrose and sodium chloride were selected as 52.4%, 46.2% and 1.4% respectively, based on similar work at frequencies of 100MHz to 1GHz reported in [7-8]. A hollow fibreglass mannequin shell of thickness 3mm was selected to contain the liquid and has a physical size and shape that closely resembles that of a human arm as shown in Figure 3(a). The phantom arm was placed on a non-conductive fibreglass tripod stand for subsequent VNA measurements as shown in Figure 3(b).

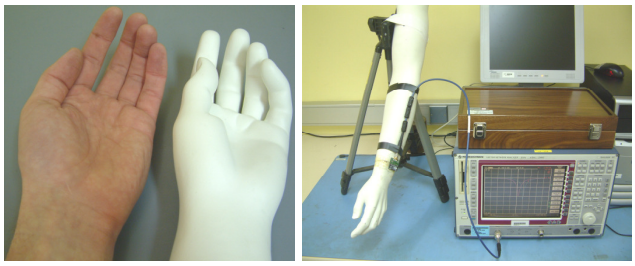

(a) (b)

Fig. 3 (a) Human and phantom hand/wrist comparison, (b) VNA test setup

During measurements, the test antenna was first placed on the phantom wrist. Several ferrite-beads were placed on the 50Ω cable to help suppress cable shield currents to improve measurement accuracy. The test antenna was then placed on the human arm with a 3mm plexiglass insulator used to model the phantom arm shell thickness and prevent contact of the back side of the antenna with the skin as skin contact has a pronounced effect on the measurement and is difficult to simulate. The impedance and return loss of the test antenna were then measured on both the phantom and human wrists and the results compared. In Figure 4(a) and (b), it can be seen that the measured antenna resistance and reactance for the human and phantom wrists are in good agreement at frequencies close to the nominal antenna resonant frequency of 433MHz, denoted f_0 in Figure 4(a).

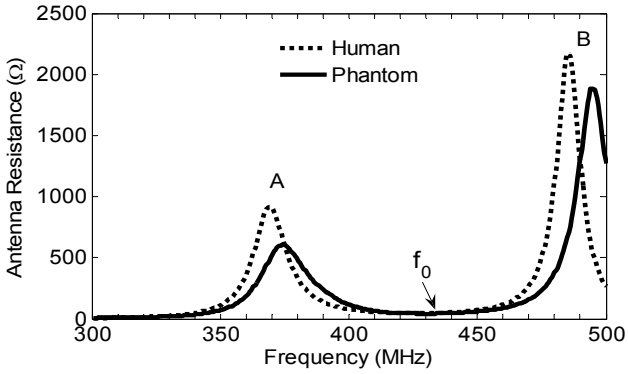

(a)

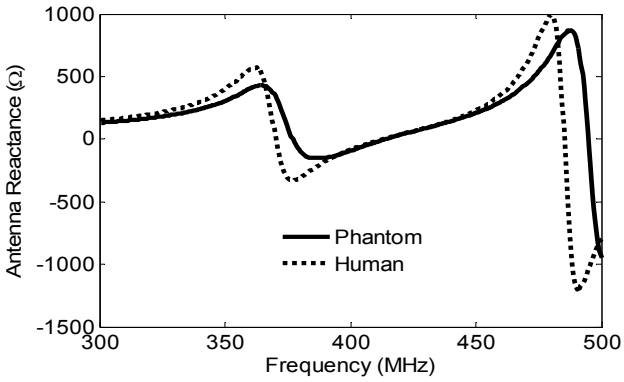

(b)

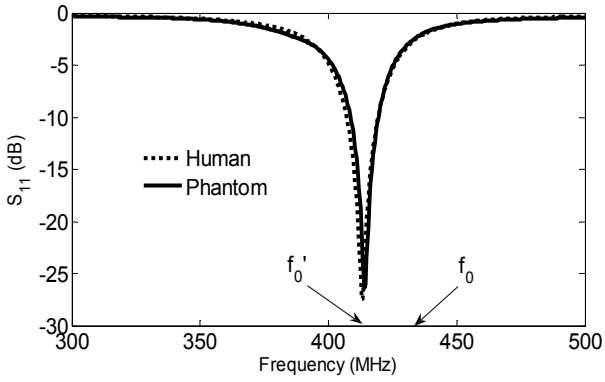

(c)

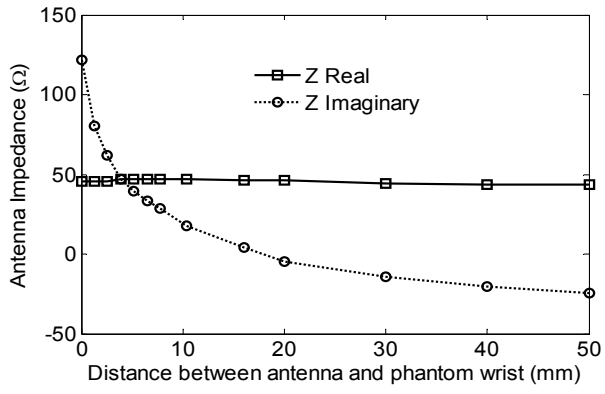

(d)

Fig. 4 (a) Antenna resistance, (b) Antenna Reactance, (c) Return Loss, (d) Variation of antenna impedance with distance to phantom wrist

Note that two resonances (A and B) were observed in the antenna resistance and reactance plots occurring at frequencies of approximately 370 and 490MHz as shown by Figure 4(a) and 4(b). The antenna impedance at these frequencies is much greater than the system characteristic impedance of 50Ω and therefore the resonant effects are not reflected in the return loss measurements. Figure 4(c) compares the measured antenna return loss for the human and phantom cases and the results are in very close agreement. Figure 4(d) plots the antenna impedance profile when the separation between antenna and phantom wrist is varied. It can be seen that the reactance of the antenna is capacitive for separations of greater than 20mm and becomes inductive for distances less than 20mm approximately. The inductive component of the antenna impedance increases dramatically for separations less than 5mm. For this particular test antenna, the real component does not vary greatly and remains in the range 42 to 46Ω approximately. A number of other antenna types were measured on the human and phantom wrist and the impedance profile (both antenna resistance and reactance) was found to vary considerably depending on the type of antenna. From the above measurements, it can be seen that the matching circuit for this antenna needs to able to match any impedance in the range of approximately 44-j24Ω to 46+j122Ω.

IV. Custom Antenna Measurement System

In this section, the design of a custom antenna measurement system is presented. The purpose was to develop a flexible, low-cost, experimental platform to investigate the effectiveness of using the mote itself as part of a return loss measurement system rather than the use of an extremely accurate but expensive VNA instrument. The other aim was to develop a flexible system that would allow the evaluation of various types of closed-loop reconfigurable antenna tuning circuits and tuning algorithms for use in wireless mote applications. The block diagram of the system is shown in Figure 5 and the blocks within the dotted section are the subject of this discussion.

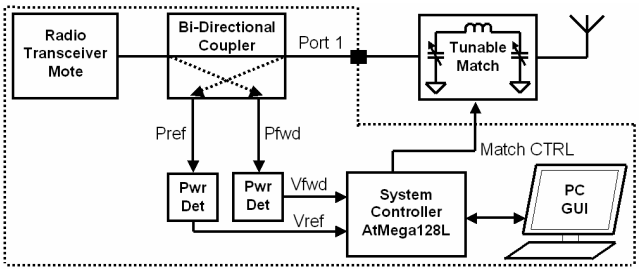

Fig. 5 Mote antenna characterization system

The radio transceiver (mote) is used as the source of RF power. During measurements, the transceiver is placed in transmit mode and is programmed to output a +10dBm single tone, continuous-wave (CW) signal at a fixed frequency of 433MHz. The transceiver is connected to the input port of a commercial bi-directional coupler [9]. The output port of the coupler (denoted Port 1 in Figure 5) is connected to a matching circuit or the input of an antenna. The coupler also provides a sample of the coupled forward power P_{fwd} as well as the coupled reflected power P_{ref} from Port 1. The chosen coupler for this application has a bandwidth of 10 to 600MHz, a low insertion loss of 0.3dB at 433MHz with coupling and directivity of 20dB and 25dB respectively and a voltage standing wave ratio (VSWR) of 1.05:1. The coupled forward and reflected powers are measured using two commercial power detectors [10] with temperature compensated DC outputs. These detectors have a wide bandwidth of 10MHz to 8GHz, a sensitivity of -55dBm to +20dBm with a low VSWR of 1.05:1.

The system controller is implemented using a low-power, high-performance, 8-bit RISC based Microcontroller [11]. The microcontroller is used to digitise the power detector outputs as shown in Figure 6. The power detectors were pre-calibrated from physical measurements to generate a lookup table to accurately compute the values of forward and reflected power denoted $P_{fwd\,(mW)}$ and $P_{ref\,(mW)}$.

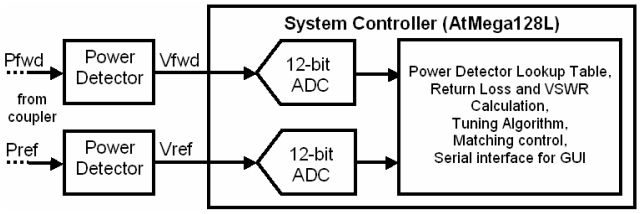

Fig. 6 Power detectors and system controller

The system controller then calculates the magnitude of the antenna reflection coefficient at port 1 as

$$|\Gamma|_{PORT1} = \sqrt{\frac{P_{ref(mW)}}{P_{fwd(mW)}}}\,. \qquad (1)$$

Knowledge of the antenna reflection coefficient is then used to calculate the return loss and VSWR at Port 1 as well as allow the tuning algorithm to determine when the matching network has been adjusted for minimum antenna reflection. A photograph of the fabricated prototype antenna characterization system is shown in Figure 7.

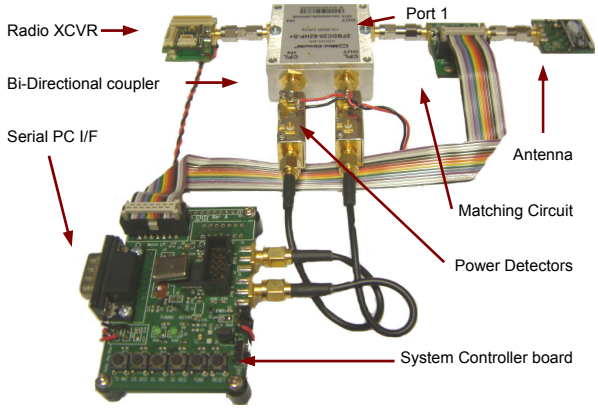

Fig. 7 Fabricated prototype antenna characterization system

The system controller board is used to perform measurements, adjust the re-configurable matching circuit and transfer the measured results to a personal computer for

display and analysis on a simple GUI. The developed GUI is a simple interface that was implemented in Labview®. An example of the user interface is shown in Figure 8(a) with parameters of interest such as measured coupler power levels, antenna VSWR, reflection coefficient and return loss displayed in graphical form in real-time.

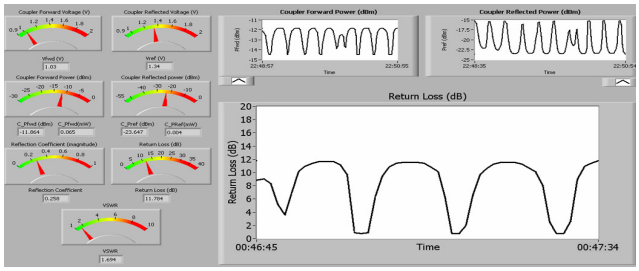

(a)

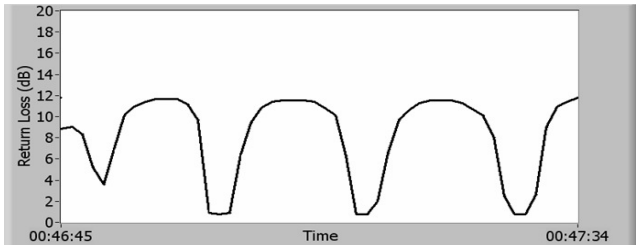

(b)

Fig. 8 (a) Screen shot of GUI, (b) Close-up of measured return loss

Figure 8(b) shows a close-up of the measured return loss when the user's hand periodically touches an antenna that has been connected to Port 1.

In order to test the accuracy of the prototype return loss measurement, a variable load impedance was applied to the output of the bi-directional coupler at Port 1. The load VSWR was swept from a value of 1.06:1 to 10:1, simulating a wide range of possible antenna mismatch conditions. For each value of load VSWR, the return loss was measured on the prototype system denoted $|S_{11}|_A$ followed by an accurate measurement using a calibrated VNA denoted $|S_{11}|_B$. All measurements were performed at a frequency of 433MHz and Table I tabulates the results.

TABLE I
COMPARING MEASURED RETURN LOSS MAGNITUDE OF THE PROTOTYPE SYSTEM VERSUS CALIBRATED VNA MEASUREMENTS (AT 433MHZ)

Load VSWR	Prototype $\lvert S_{11}\rvert_A$ (dB)	VNA $\lvert S_{11}\rvert_B$ (dB)	Error $\lvert S_{11}\rvert_B - \lvert S_{11}\rvert_A$ (dB)
1.06:1	-33.01	-30.26	2.75
1.49:1	-14.01	-14.11	-0.10
2.00:1	-9.08	-9.27	-0.19
4.00:1	-4.54	-4.38	0.16
6.00:1	-3.03	-2.85	0.18
8.00:1	-2.43	-2.16	0.27
10.00:1	-1.99	-1.73	0.26

It can be seen that the prototype and VNA return loss measurements are in very good agreement across a wide range of load VSWR values. However, for values of VSWR close to 1:1 (30dB return loss approximately), the difference between the two measurements increases significantly and is most likely due to the finite directivity of the bi-directional coupler (25dB) that sets a limit of the return loss that can be measured [12].

V. CONCLUSIONS

This paper presented the results of an investigation into antenna detuning on wireless devices caused by the presence of the human wrist. A low cost human phantom arm was developed and characterized that accurately simulates human tissue at 433MHz frequencies. The measured antenna impedance and return loss results can be used in the design and simulation of impedance matching circuits. A flexible and low cost, 433MHz antenna measurement system was also developed and characterized to measure antenna return loss. The accuracy of the system has been verified by comparing the measured results to accurate calibrated VNA measurements. The developed system is currently being used as a platform for evaluating various types of closed-loop reconfigurable antenna tuning circuits and tuning algorithms for energy efficient wearable wireless mote applications.

VI. ACKNOWLEDGMENT

We would like to acknowledge the support of Enterprise Ireland for funding this work under Grant PC_2008_324.

REFERENCES

[1] K. D. Wise, "Wireless integrated microsystems: Wearable and implantable devices for improved health care", 15th International Conference on Solid-State Sensors, Actuators and Microsystems, art. no. 5285579, pp. 1-8, 2009.

[2] Y. Lee, W. Y. Chung, "Wireless sensor network based wearable smart shirt for ubiquitous health and activity monitoring", Sensors and Actuators, B: Chemical, 140 (2), pp. 390-395, 2009.

[3] B. O'Flynn., S. Bellis., K. Delaney., J. Barton., S. C. O'Mathuna., A. M. Barroso, J. Benson., U. Roedig., and C. Sreenan., "The Development of a Novel Miniaturized Modular Platform for Wireless Sensor Networks", Proc of 5th International Symposium on Info Processing in Sensor Networks (IPSN/SPOTS), Apr. 2005.

[4] Wang, Z., Chen, X. and Parini, C.G., "Effects of the Ground and the Human Body on the Performance of a Handset Antenna", IEEE Proc. Microwave & Antenna Prop., Vol. 151, No. 2, pp. 131-134, 2004.

[5] K.L. Wong and C.I. Lin, "Characteristics of a 2.4-GHz compact shorted patch antenna in close proximity to a lossy medium", Microwave Opt Technology Letters, pp. 480–483, 2005.

[6] AntennaFactor, Product Data Sheet, ANT-433-SP, 2008.

[7] Ogawa, K., Matsuyoshi, T., Iwai, H., Hatakenaka, N., "A high-precision real human phantom for EM evaluation of handheld terminals in a talk situation", IEEE Antennas and Propagation Society, AP-S Int Symposium (Digest), 2, pp. 68-71, 2001.

[8] P. Liu, C. Rapaport, Y. Z. Wei and S. Sridhar, "Simulated Biological Materials at Microwave Frequencies for the Study of Electromagnetic Hyperthermia," IEEE EMBS Digest, V, pp. 272-273, 1992.

[9] Minicircuits, Product Data Sheet, ZFBDC20-62HP+, 2009.

[10] Minicircuits, Product Data Sheet, ZX47-55+, 2009.

[11] Atmel, Product Data Sheet, Atmega128L, 2009.

[12] R. White, *Spectrum and Network Measurements*, PTR Prentice Hall, New Jersey, 1993.